by B. J. Rubin

An electromagnetic approach for modeling high-performance computer packages

Described here is an electromagnetic approach for the analysis of high-performance computer packages such as the thermal conduction module (TCM) used in the IBM 3080 and 3090 processor units. Modeling of signal paths and limitations of previous methods are discussed. Numerical results are presented for propagation characteristics associated with signal lines and vias, and for coupled noise between signal lines. The results are compared with those obtained by means of test vehicles, scale models, and capacitance calculations.

[®]Copyright 1990 by International Business Machines Corporation. Copying in printed form for private use is permitted without payment of royalty provided that (1) each reproduction is done without alteration and (2) the *Journal* reference and IBM copyright notice are included on the first page. The title and abstract, but no other portions, of this paper may be copied or distributed royalty free without further permission by computer-based and other information-service systems. Permission to *republish* any other portion of this paper must be obtained from the Editor.

Introduction

For early computers there was little need for a sophisticated model of the module-level or card-level wiring used to interconnect computer circuits. The rise times of the waveforms generated by the circuits were either many times the propagation delay between the circuits, or the machine cycle time was so large that multiple reflections of the signal waveforms in the module-level and card-level wiring were permitted. For the former, the various signal-line reflections which occurred did so within the rise time; for the latter, the receiver output was sampled after the reflections subsided. In either case, the capacitance and perhaps series resistance of the signal-line segments were the only parameters that needed to be characterized. In more recent computers [1-3], such as the IBM 3080 and 3090, rise times are often much shorter than the propagation delay between circuits on different chips. Furthermore, to avoid delay penalties that would impact the cycle time, receivers must switch at the first incidence of the signal

waveform and not after multiple reflections have occurred. This has led to a number of package-related concerns [4].

Specifically, because of the short rise times, the reflections have become distinct. The amplitudes of these reflections must be minimized so that they do not cause receivers to switch falsely [4]. Accordingly, the signal lines must be treated as transmission lines, and the various connections to them, such as stubs and vias, must be treated as discontinuities. Appropriate models, mostly involving the use of distributed *RLC* networks, have been used to represent the signal lines; and lumped networks have been used to represent the various discontinuities that are present along the signal paths.

Furthermore, the shorter rise times lead to an increase in the noise which is coupled between driven and quiet signal lines. Such noise or crosstalk, due to the parasitic coupling between neighboring signal lines, must be taken into consideration to avoid false switching of receivers on the quiet lines [4]. In addition, the signal waveforms on a line are also affected by nearby conductive elements, such as vias and other signal lines which may not be in direct contact with the line. Such other lines and vias (OLVs) slow the propagation of signals by increasing the inhomogeneity of the signal-line environment and affecting associated impedances and coupling parameters. Thus, the electrical design of a computer package generally requires information regarding

- Propagation delays and characteristic impedances associated with the signal lines.
- Equivalent circuits for the stubs and other discontinuities which may be present.
- Propagation delays and impedances associated with the vias.
- Crosstalk between the signal lines.
- Changes in the above resulting from the presence of OLVs.

In an effort to model these effects, some excellent computer programs have been developed. The programs calculate the capacitance, inductance, and resistance of two-dimensional signal lines [5, 6] and their three-dimensional discontinuities [7, 8]. Virtually any geometry of interest can be analyzed, and most of the few remaining restrictions are being removed through continuing refinements in the programs. Because accuracy is limited only by the numerical grid size specified by the user, which in turn is limited by the computer resources available, highly accurate circuit models can be obtained. This circuit approach, however, has some fundamental limitations.

In a circuit model, all coupling effects appear instantaneously; they do not display the true physical

time retardation associated with the finite velocity of light. To correctly model structures having transverse dimensions comparable to the wavelengths that compose the signal waveform, significant modifications such as the inclusion of retarded effects may be required [9]. Further, a discontinuity modeled through lumped elements contains various electrical nodes at which the circuit elements are connected. This artificial constraint of forcing current to flow through nodes is often not suitable for structures where current flow and coupling are distributed over large areas. A further difficulty is that both capacitive and inductive models must be generated and then merged; the resulting LC model may be unduly complex.

For example, consider a perfectly conducting signal line having uniform cross section and situated in a homogeneous medium above a ground plane. Such a structure is known to support a transverse electromagnetic (TEM) wave, viz., no electric or magnetic field components exist along the direction of propagation, and the wave travels at the velocity of light in the dielectric [10]. The equivalent circuit of this structure is a uniform transmission line having per-unitlength capacitance C and per-unit-length inductance L; absolutely no coupling is present. Yet a model generated by sectioning the structure along its length and using 3D capacitance and inductance calculations would display coupling capacitances and inductances between all sections. If the structure were recognized as supporting a TEM wave, the self and coupling capacitances could be merged, as could the inductances, with the final result being the same C and L discussed above. When discontinuities are introduced along the signal line, however, the structure will no longer support a purely TEM wave. In many cases the geometry and frequency range are such that, to within engineering accuracy, the above merging of circuit elements is still justified. In other cases, where signal lines meander and perhaps run over holes in the ground plane or run near large floating conductors, the sections may be so tightly and intricately coupled that it is not worth the time and effort even to attempt simplification. Provided that the circuit model, after any required modifications, is valid, the preferred course of action may be to leave the model in its unsimplified and thus unduly complex form. Another concern is the zero gap between adjacent sections of the same conductor, which may cause difficulties in calculating associated capacitances and require that the model be carefully generated.

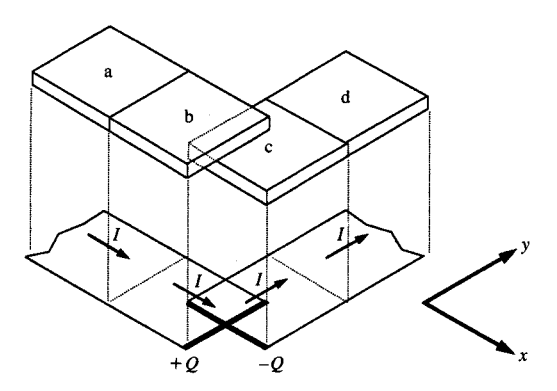
The above LC modeling approach, despite its limitations, has been and will almost certainly continue to be a primary means for the analysis of computer packages. The package geometries and frequencies associated with today's, and even projected, systems in

most cases can be accommodated by the LC approach. Nevertheless, to provide solutions at the higher frequencies, to handle unconventional package structures not especially suited to circuit approaches, or to handle non-TEM structures such as waveguides and their discontinuities, alternative techniques must be developed. One alternative involves the use of a *full-wave* electromagnetic analysis (the term *full-wave* refers to a rigorous use of Maxwell's equations). Thus, all coupling and retarded effects are implicitly included. We now describe such an approach, based in the frequency domain, and use it to model a high-performance TCM. In the following, the time dependence is $e^{j\omega t}$, where ω is the angular frequency and t is time.

Electromagnetic approach

Though numerous approaches exist for electromagnetically modeling three-dimensional structures, the author has selected one that employs a current expansion and moment-method techniques [11]. To make use of this approach, four steps must be taken. First, a suitable set of basis functions must be chosen. The current is expressed through a linear combination of coefficients (which serve as the unknowns) multiplied by these basis-function elements. Second, an appropriate field quantity, such as, in this case, electric field, must be expressed as a function of the current density, and thus in terms of the unknown coefficients. Third, a test criterion must be decided upon and applied in a sufficient number of ways to generate a matrix equation. If P current basis functions and thus P unknown coefficients exist, P independent tests are generally performed. In our case we choose to apply the electric field boundary condition, namely that the tangential component of electric field vanishes over P regions of a lossless conductor. Fourth, the resulting P-by-P matrix equation must be solved for the current, which in turn can be used to find equivalent electrical parameters.

This procedure is quite similar to that which has been used in 3D capacitance algorithms [7]. There, charge is represented as a linear combination of 2D pulse basis functions. The voltage, in terms of the unknown coefficients of the basis functions, is evaluated at a sufficient number of locations to generate a matrix equation. The solution of the matrix equation is the charge density, which is then used to obtain the capacitances. The 2D pulse functions are subsectional, since each is nonzero over a different rectangular region. Such subsectional basis functions facilitate the representation of irregularly shaped structures; they are used in a manner analogous to tiles covering an oddshaped floor. As described shortly, a similar but smoother set of basis functions is preferred for the electromagnetic approach.



Finnire

Approximation of current bending around a corner by means of pulse functions.

Though only currents are involved, the charge and all its related effects are implicitly included and related to the current through the continuity equation [10], which for current flowing on a surface may be expressed as

$$\nabla \cdot \mathbf{J}_{s} = -j\omega \rho_{s},\tag{1}$$

where J_s is the surface current density and ρ_s is the surface charge density. We assume that the conductors are embedded in a homogeneous dielectric medium. Furthermore, the conductors are assumed to be lossless; thus, current flows only on the outside surfaces of the conductors, so that the internal regions need not be considered. We next discuss the four aspects of the electromagnetic solution.

Selection of basis functions

The basis functions that represent the current must be carefully chosen so that the calculated current distribution approximates the true physical flow. Consider, for example, the L-shaped section of conductor shown in Figure 1, where current bends around the corner of the L. In this example, we are not interested in the exact details of the current flow; rather, we simply want to examine what happens when different basis functions are used to approximate the current distribution. To do so, we first try to approximate this current flow through a linear combination of 2D pulse functions.

Over each rectangular region that a pulse function covers, the current flows in one direction and has a constant value given by its coefficient. Outside the

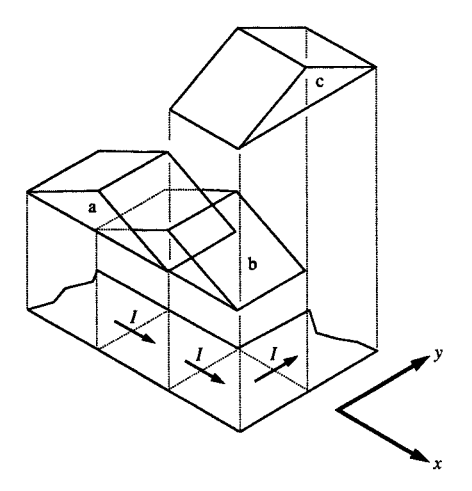
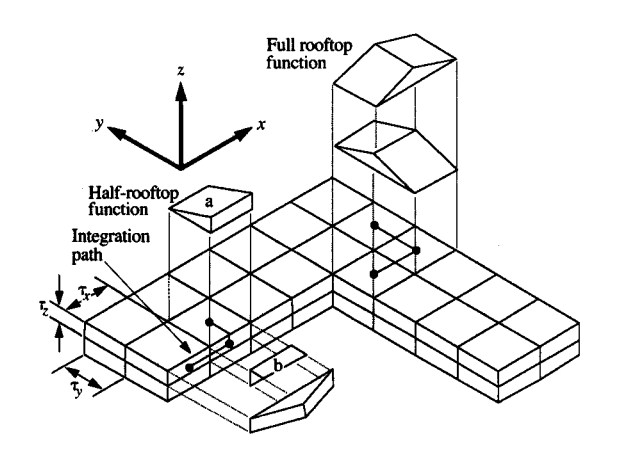


Figure 2

Approximation of current bending around a corner by means of rooftop functions.



Britte

Section of a unit cell showing rooftop function elements and integration paths for a mesh plane. From [19], reproduced with permission; © 1989 IEEE.

rectangular region, the current is zero. Because the current flow is two-dimensional, sets of x-directed and y-directed pulses are required. The x and y sets of pulses may overlap, or may be offset as in Figure 1.

Independent of any offset, for current to change from the x to the y direction, or in other words bend around a corner, the current along x must discontinuously end and then continue again in the y direction. As shown in Figure 1, x-directed pulse functions a and b, and y-directed pulse functions c and d, each carry a current I. As dictated by Equation (1), line segments supporting a total charge (also shown in the figure) $O = I/i\omega$ are generated. Because such charge is fictitious (it does not physically exist), the electromagnetic field it produces may lead to erroneous results. This is especially true at low frequencies, where charge is the dominant contributor to the electric field. Though a procedure for representing the current and testing the field using pulse functions could perhaps be developed that would avoid such pitfalls, it is not clear that the procedure would work in every case. To avoid potential problems, the rooftop basis function [12], which has a triangle shape in one direction and a pulse shape in the other direction (Figure 2), is chosen.

From Equation (1) and the mathematical description of the rooftop function given in the Appendix, a rooftop function that carries a current I gives rise to two charges, uniformly distributed over adjacent rectangular areas. The first is -Q, which appears over the rectangle associated with the rising half of the rooftop function, and the second is +Q, over the rectangle associated with the falling half. Because the charges associated with the x-directed rooftop function b and y-directed rooftop function c are equal and opposite over the rectangle where they overlap, no fictitious charge results. The smoother shape and overlap (as many as four rooftop functions may overlap a given rectangular region) give rise to this more physical representation. These rooftop functions are perhaps the simplest functions that adequately model the physical current in typical computer packages.

The rooftop functions are placed over each conductive surface. At corners, where half-rooftop functions exist, corresponding half-rooftop functions are combined (by making their coefficients dependent) to form corner functions, as are half-rooftop functions a and b in Figure 3. Current is continuous around corners, preventing artificial line charges at edges. A further choice must be made regarding the boundary conditions of the structure that is to be modeled.

We would like to calculate the propagation characteristics of a signal-carrying structure that is not obscured by the presence of source or termination regions. Such end regions, being electromagnetically coupled to the rest of the structure, modify its propagation characteristics. For instance, it would be difficult to determine how much of the inductance is due to a signal line and how much is due to its attached

source and termination. Furthermore, the variations in the shape or other attributes of the end regions would inevitably yield some difference in results; considerable interpretation might be required to extract the correct signal-line parameters. The author chooses to enforce periodic boundary conditions so that end regions need not be included.

A region of the original structure is selected and periodically repeated along the x and y directions; the repeated region is designated as a unit cell. We now choose and in fact force the direction of propagation to be in the x direction by representing the current in each unit cell by the same linear combination of rooftop functions that is further multiplied by $e^{-jk_x x}$. The parameter k_{ij} is referred to as the propagation constant and essentially gives the propagation velocity of the wave. The current distribution, which is a periodic function multiplied by the above exponential factor, automatically satisfies Floquet's (Bloch's) theorem [13] and is thus a legitimate choice. Further, because the above exponential dependency is precisely that expected in a TEM structure and roughly that expected in many quasi-TEM structures (which include most computer packages), it makes sense to include this factor explicitly. The unit cell must include at least two paths continuous along the x direction so that signal and return current can flow along the x direction.

The periodicity along the x direction is necessary for waves to propagate. The periodicity along the y direction, however, gives rise to coupling between unit cells that is generally undesirable but can be minimized. For instance, if we wish to analyze an isolated signal line above a mesh plane, we define a unit cell having a y-periodicity much greater than the height of the signal line above the mesh plane; thus, the coupling between signal lines in neighboring unit cells is small. If we wish to model two adjacent signal lines that run parallel along the x direction, we may define a unit cell that has three adjacent signal-line channels and leave one of these channels vacant. Thus, coupling is essentially limited to those adjacent lines that reside within the same unit cell.

Expressing and testing the electric field

The electric field is calculated using Maxwell's equations and facilitated, because the structure is periodic, by a Fourier analysis. The process is described in [14–16] for structures composed of conductors that have zero thickness and lie in the x-y plane, and in [17] for 2D signal lines that have cross sections lying in the x-z plane. For general 3D structures the process is more complicated, because rooftop functions may lie in the x-y, y-z, and x-z planes. Once expressed, the electric field is then tested by integrating the electric field over line intervals that overlap the rooftop functions (Figure

3). This involves satisfying the electric field boundary condition

$$\mathbf{E}_{t} - \mathbf{J}_{s} R_{s} = 0, \tag{2}$$

where \mathbf{E}_{t} is the tangential electric field and R_{s} is either a surface or sheet impedance associated with the conductor. For perfect conductors, R_{s} is zero. Line intervals were chosen because at the same time they provide, through Maxwell's equations, a test of the normal component of magnetic field wherever four line intervals form a closed rectangle. This consequence is believed by the author to yield stability in the numerical solution at low frequencies. By forcing the tangential component of the electric field to vanish over each rooftop function, we obtain a matrix equation having the form

$$\mathbf{Z}(k_{\nu})\mathbf{I} = \mathbf{0},\tag{3}$$

where I is a column vector of current coefficients having length P and Z is an order-P matrix of impedances. For the convenience of the reader, a derivation of the elements of the Z matrix is given in mathematical detail in the Appendix.

Solving the matrix equation

To find the current, we first recognize that the matrix equation (3) represents an eigenvalue problem, with k_x as the eigenvalue and I as the eigenvector. The values of k_x that satisfy Equation (3), from elementary linear algebra, are those for which the determinant of \mathbf{Z} vanishes. A Newton search [15] may be used to find k_x . Substitution of k_x back into Equation (3) gives I.

For structures involving only a single signal line and one reference conductor (that is, two nontouching conductors that are continuous along the x direction), only one quasi-TEM solution exists. (A reference conductor, which represents a return current path, must be specified to guarantee that transmission line propagation can exist.) If multiple signal lines are present, as is the case in a crosstalk analysis, multiple solutions generally exist [16]. The current distribution associated with each different propagation constant is referred to as a mode. For a structure consisting of N noncontacting conductors that are continuous along the x direction, in general N-1 quasi-TEM modes are possible. The actual solution consists of that linear combination of modes that satisfies the boundary conditions at the source and termination regions. This is analogous, for N=3, to a circuit having two independent capacitances, where two modes (exponential in shape) are possible. The charges initially stored on the capacitors determine how much of each mode appears in the circuit's output response. If, however, multiple reference conductors exist (which occurs, for example, when two or more mesh planes

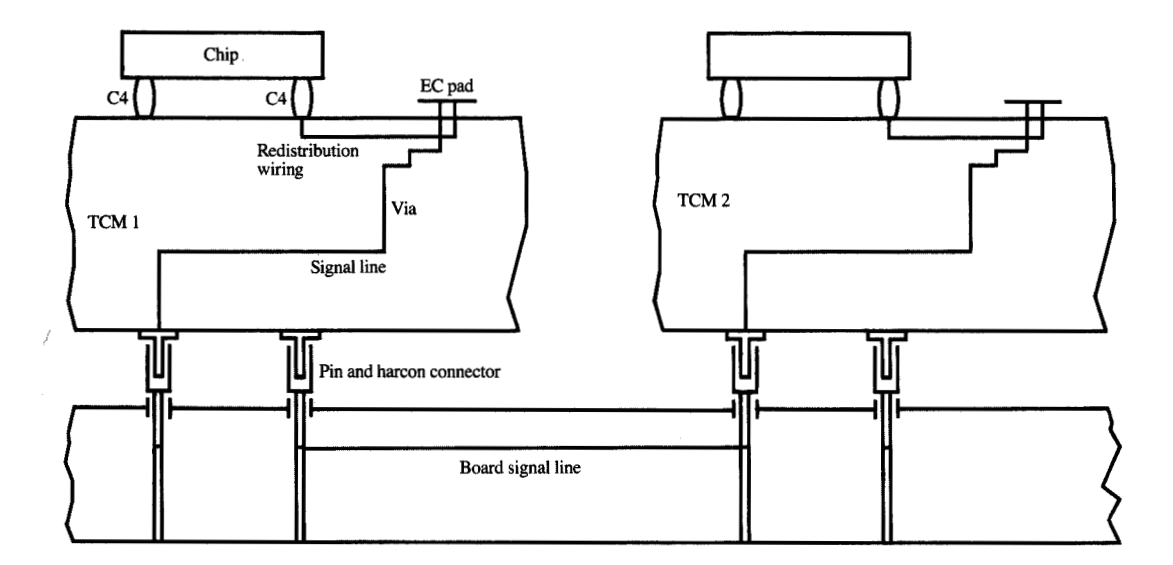


Figure 4

Illustrative view of chip-TCM-board configuration showing electrical connections. From [20], reproduced with permission.

surround a signal line), they must be shorted together through conductive straps to preclude the presence of such multiple (and undesirable) modes. (In practice, such modes are precluded because the mesh planes of a TCM are tied together either directly through vias or indirectly through paths that may include vias, pins, circuits, and capacitors.)

For most computer package structures, the nature and distribution of the discontinuities are such that the curve for propagation constant vs. frequency, known as the dispersion curve, is linear up to and beyond the highest frequency of interest; only one frequency needs to be considered. Thus, the propagation velocity ν is equal to the phase velocity of the propagating wave, ω/k_x ; the propagation delay t_0 relative to that of light may be expressed as $t_0 = c/\nu$, where $c = 1/\sqrt{\mu_0 \varepsilon}$ is the speed of light in the dielectric medium, μ_0 is the permeability of free space, and ε is the dielectric constant of the medium. Voltages, which for non-TEM structures are pathdependent, may be found by integrating the electric field. Effective values of per-unit-length capacitance C and perunit-length inductance L may be calculated, for lossless structures, through $t_0 = \sqrt{LC}$ and $Z_0 = \sqrt{L/C}$, where Z_0 is the characteristic impedance (defined in the Appendix). For structures involving multiple signal lines, the

propagation constants and associated current and electric field distributions may be used to find the capacitance and inductance matrices, and the near- and far-end coupled noises [16].

An equivalent circuit model for a finite size discontinuity can be inferred from computations performed on two signal-line models, one having the discontinuity and the other not. The electrical model of a stub, for instance, could be obtained by analyzing two distinct signal-line structures, one with stubs and the other without. The differences in capacitance and in inductance are due to the stub, and represent its excess capacitance and inductance. This procedure of tying a discontinuity to a signal line is physically justified, since the surrounding environment of the discontinuity must be taken into account. Almost any computer package structure can be represented through a unit cell for subsequent analysis.

In the following, we are not concerned with such details as the number of Fourier series terms used to find the matrix elements, the numerical grid required to obtain accurate results, the details of the Newton search to find the propagation constants, the paths used to define the voltages, or the computer code employed. These issues have been considered in detail in [14–19].

590

What we do concentrate on here are the salient packagerelated features of this electromagnetic analysis. This includes defining appropriate unit cells, adequately specifying the problem, and interpreting associated numerical results. The accuracy of the approach will become evident from a comparison of results to those obtained through scale model and test vehicle measurements.

Description of package used in the analysis

The TCM [2] used in the IBM 3090 is a 10-cm-square substrate which contains 36 conductive, molybdenum layers in an alumina dielectric; the substrate contains the signal wiring and power distribution to support 100 chips that are mounted on its surface. Illustrative portions of a chip-TCM-board configuration are shown in Figure 4, where chips on two TCMs are interconnected through a path that includes C4 solder balls, engineering change (EC) pads, vias, signal lines, harcon connectors, and pins. The C4 solder balls provide the connections from the chip input/output (I/O) pads on the surface of the chip to surface pads on the TCM. A short length of via ties a surface pad to the redistribution path, which includes signal-line segments and vias. This redistribution wiring serves as a space transformer to connect the chip's power pads and 96 signal I/O pads, which lie on a partially dense 0.25-mm grid, to the vias and signal lines in the TCM that lie on a 0.5-mm grid. The EC pad allows for voltage test measurements. Through laser deletion of its attached delete pad and subsequent bonding operations to insulated wires, engineering changes can be made. The next section of via provides connection to the signal line, which may proceed to another chip site on the same module, or to a chip site on a different module, as shown. The harcon and pin serve as the connection between TCM and board. The various aspects of the package are discussed in more detail in [2, 3]. We concentrate here on the signal-line region, which includes signal lines, vias, and mesh reference planes.

Figure 5 focuses on the signal wiring, showing a signal line, situated between mesh reference planes, that is connected to a second signal line through a via. (It is more typical, though, for such vias to interconnect x and y signal lines that are situated between the same mesh reference planes.) The various structures are shown as rectangular because the analysis technique requires that the structure be defined by steps along the Cartesian axes. For the TCM used in the 3090, the signal pitch $d_{\rm m}$ is 0.5 mm. Signal lines have width w=0.1 mm and thickness t=0.025 mm. The mesh plane segments, which are aligned with the signal lines so that their projections on the x-y plane coincide, are assumed to have the same dimensions. The vias are centered in the mesh plane openings, and for the sake of analysis, are approximated

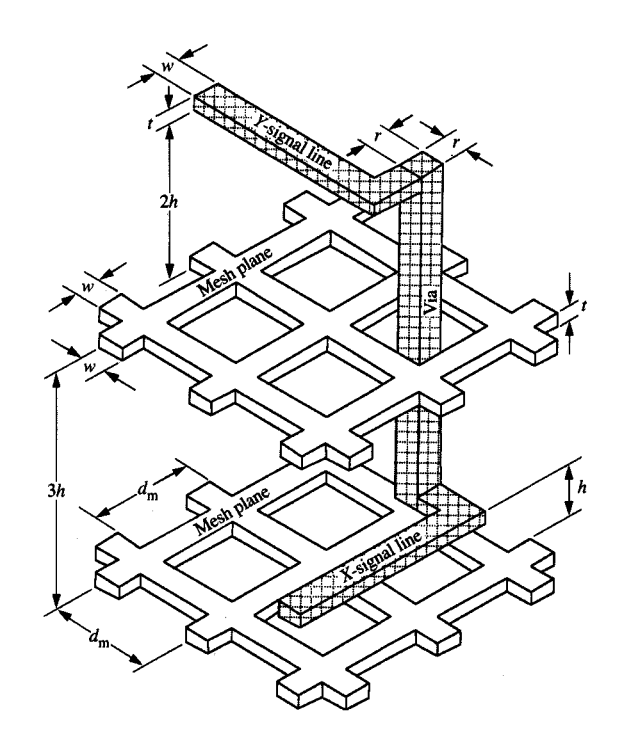


Figure 5

Section of TCM showing reference planes and signal lines interconnected through a via. From [19], reproduced with permission; © 1989 IEEE.

as squares with side r = 0.15 mm. Vertical spacing h is 0.2 mm, and the relative dielectric constant is 9.5. The set of structures we now describe has not been previously analyzed, either through circuit-based or other techniques.

Structures analyzed

The basic signal-line structure, as shown in Figure 5, involves a signal line between two mesh reference planes. To minimize unwanted coupling to nearby signal lines, the unit cell includes two vacant signal-line positions. For modeling purposes and if present, the adjacent vias and crossing signal lines that constitute the OLVs appear periodically, unless otherwise noted, at every available unfilled position within the unit cell. For instance, a given signal line could have 20 crossing y signal lines per cm, and as many vias on each side. Because we assume lossless conductors, the eddy currents (and thus magnetic field) within the molybdenum conductors are not modeled. Inductance will be smaller, and other

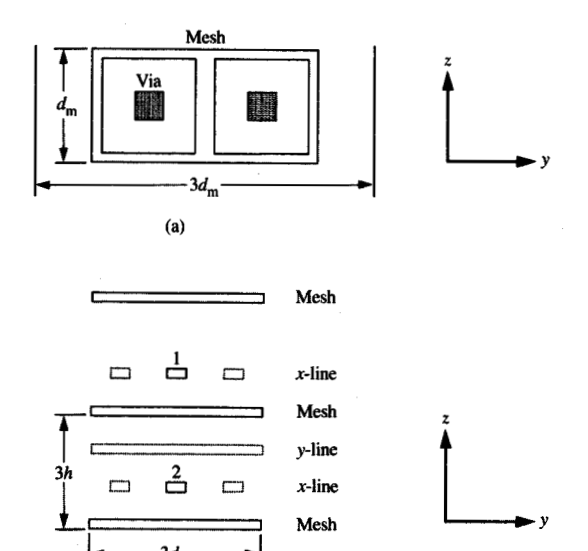


Figure 6
Unit cells for (a) via and (b) vertical signal-line coupling.

(b)

propagation parameters related to the inductance will be affected accordingly.

To calculate the propagation parameters of the via, a structure that supports propagation must be modeled. We thus consider a via that runs through an infinite array of mesh planes; the unit cell is oriented with x along the length of the via, and y and z as shown in Figure 6(a). The unit cell must contain two vias, one of which carries the signal current and the other the return current; a quasi-TEM wave cannot propagate on a single via. Only part of the mesh plane is included, to reduce the number of current elements required for the analysis, and a buffer region that contains no vias is used to reduce coupling between unit cells adjacent along the y direction. Since the propagation parameters are somewhat sensitive to the return via location, and since return vias cannot always be identified in actual packages, some differences between calculated and measured parameters may result. For instance, when a via is more distant from other vias, its capacitance decreases and its inductance increases.

For coupled noise calculation, unit cells must include the signal lines of interest and surrounding mesh planes. (Mesh planes only imperfectly shield signal lines located on opposite sides.) The unit cell for coupling between two signal lines vertically separated by a mesh plane is shown in Figure 6(b). Here, three mesh planes are modeled, and some signal-line (shown dashed) positions are intentionally left vacant so that coupling is reduced between unit cells adjacent along the y direction. Signalline positions 1 and 2 only are occupied. For the cases that involve horizontally or diagonally coupled signal lines, the unit cells are four signal pitches (or 2.0 mm) wide, and include respectively two and three mesh planes. For diagonal coupling, signal-line position 1, for instance, would be shifted a distance $d_{\rm m}$ along the y direction. For horizontal coupling, two adjacent signal-line positions at the same height would be occupied. When present, vias occupy only the positions between the signal lines for the horizontal coupling case.

To find the coupling parameters for any of these two-signal-line structures, it is necessary to find the two possible solutions or modes, as discussed earlier, and then to apply the procedure given in [16]. In that procedure, the propagation constants, total signal-line currents, and associated signal-line voltages are used to find effective values for the capacitance and inductance matrix elements. For the horizontally coupled configuration, where the structure involves only two signal lines and is symmetric along the y direction, an even-mode, odd-mode analysis [19] can be used instead. The saturated near-end noise, $V_{\rm NE}({\rm sat})$, expressed as a percentage of the signal swing, for instance, can then be approximated as

$$V_{\rm NE}({\rm sat}) = 0.25 (C_{12}/C_{11} + L_{12}/L_{11}),$$

where C_{11} and C_{12} are appropriate self and coupling capacitances, and L_{11} and L_{12} are appropriate self and mutual inductances.

For all of the analyses, the mesh planes must be shorted together with conductive straps (not shown) for reasons discussed earlier. The OLVs, if present, are also shorted to a mesh plane. For the signal-propagation cases, the mesh planes, as well as any y-lines that may be present, are shorted together by a 0.1-mm-wide rectangular strap which lies in the x-z plane; the vias, if present, are shorted to the uppermost mesh plane by a 0.025-mm-high rectangular strap that lies in the y-zplane. Such straps are positioned to minimize any loading, though slight effects inevitably result. The numerical grid, which determines the number of rooftop function current elements that represent the structure, is chosen to be the coarsest one that fits the structure. The symmetry along the y direction, which is present in all but the diagonal coupling case, is used to reduce the size of the Z matrix. To allow for a coarser grid, in the signal propagation cases, the 0.15-mm-square via is offset along the x direction by 0.025 mm; in the horizontal coupling case, it becomes a 0.1-mm-square via which is offset along the x direction by 0.05 mm. A computer program has been written to perform the electromagnetic algorithm for any structure that can be defined through steps along the Cartesian coordinates.

Numerical results

Table 1 gives the propagation characteristics of the signal lines and vias in the TCM used in the IBM 3090. The propagation delay, t_0 , was normalized to the delay of light in the dielectric. The coupled noise is given for the three cases of horizontally, vertically, and diagonally adjacent signal lines; a pulse having an amplitude of 1 V and a rise time of 1 ns was considered, and (conventionally) all signal lines were assumed to be terminated in their characteristic impedance. As indicated by the column labels, the signal environment may include y-lines and/or vias. The far-end coupled noise $V_{\rm NE}({\rm sat})$ were maximum when OLVs were respectively present and not present.

The vias had a lower impedance but greater propagation delay than the signal lines. The delay was not as great as one might expect, however. The additional capacitance added by running through mesh planes is offset by a reduction in inductance caused by the eddy currents that flow around the segments of the mesh plane. If the analysis had included mesh-plane resistivity, however, these eddy currents would have been reduced (depending also on the frequency) and the delay would have been greater. When adjacent y-lines were introduced, which corresponds to signal lines running close to the via, delay was increased by 5% and impedance was reduced by about 4%.

The signal lines support waves that are nearly TEM. Even with no OLVs, though, the mere presence of mesh, as opposed to solid, reference planes caused propagation delay to exceed the TEM value by 2%. A full array of crossing y-lines increased the delay to 1.06, while the full complement of vias increased delay to 1.10. A saturation effect was noted, since the presence of both vias and y-lines increased the delay to only 1.11. The corresponding values of Z_0 , C, and L are also given in the table.

For the coupled noise, OLVs were considered only for horizontally adjacent lines. The near-end noise was greatest for horizontally coupled lines, and least for diagonally coupled lines. When OLVs were present, the near-end noise decreased by 41%, but the far-end noise increased by 315%. Since near-end noise is proportional to the sum of the capacitive and inductive coupling coefficients, while far-end noise is proportional to their difference [21], these results make sense. TEM structures have capacitive and inductive coupling coefficients that are equal. OLVs are, from calculation and from measurements, known to reduce capacitive coupling dramatically, but to reduce the inductive coupling only minimally. Thus, near-end noise could be cut in half, while far-end noise could increase considerably from zero. The above results, where possible, were compared to measurements on test vehicles and scale models, and to capacitance calculations.

Table 1 Propagation parameters for TCM used in the IBM 3090 processor unit.

Parameter	No OLVs	y-lines	Vias	All
via t ₀ (norm)	1.12	1.17	_	_
via $Z_0(\Omega)$	28.0	26.9		
via C (pF/cm)	4.12	4.48	_	_
via L (nH/cm)	3.23	3.25	_	_
$sig t_0$ (norm)	1.02	1.06	1.10	1.11
$\operatorname{sig} Z_0(\Omega)$	45.4	43.4	40.5	39.8
sig C (pF/cm)	2.31	2.51	2.79	2.87
sig L (nH/cm)	4.76	4.73	4.57	4.55
hor $V_{NE}(\text{sat})$ (%)	3.64		_	2.16
hor $V_{\rm FE}$ (mV/cm)	-1.01	_		-4.19
vert $V_{NE}(\text{sat})$ (%)	0.98	_	_	
vert $V_{\rm FE}$ (mV/cm)	-0.82	_		_
diag $V_{\rm NE}({\rm sat})$ (%)	0.55		_	_
diag $V_{\rm FE}$ (mV/cm)	-0.49	_	******	_

Comparison of calculated and measured results

The comparison is presented in **Table 2**, where the parameters calculated using the method described here are listed in the column labeled "Electromagnetic." Measurements on the test vehicles included those for signal-line and via capacitance, signal-line impedance, signal-line coupling capacitance and coupled noise, and OLV effects. Measurements on the scale models included those for via capacitance, signal-line capacitance, and OLV effects. The capacitances, characteristic impedance (from time-domain reflectometry measurements), and near-end coupled noise were chosen for comparison purposes because they could be trusted and readily measured. For the 2D capacitance analysis, the transverse conducting elements could not be included; capacitances were smaller than expected, impedances were greater than expected, and coupling parameters, because of reduced shielding, were also greater than expected. These capacitances may be viewed as bounds, and do indeed appear that way when compared with corresponding data in the other columns. The scale models, because of practical considerations in their fabrication, were only reasonable facsimiles of those TCM regions which were electromagnetically modeled. Nevertheless, the differences were relatively minor, and this column should be given the heaviest weight. Because of process variations, the test vehicle measurements should be given less weight.

Both a signal-line scale model (shown in Figure 7) and a via scale model (not shown) were constructed. The first model included round vias that contained, consistent with actual TCMs, bulges which increased OLV capacitance but which were not included in the analysis. End effects, associated with a scale model's finite size,

Table 2 Comparison of calculated and measured propagation parameters.

Parameter	OLVs	C(2D)	Electromagnetic	Scale models	Test vehicle (1979)	Test vehicle (1985)
,	none		4.12°	3.50	3.15-3.29	3.48-3.56
	y-lines	_	4.48°	_		3.77-3.81
	x,y-lines	_		4.23		_
sig C (pF/cm)	none	2.21	2.309	2.404	2.25-2.38	2.20-2.36
	y-lines		2.514	2.654	_	
	vias		2.791	2.807		_
	all	_	2.869	2.942	2.41-2.68 [†]	2.51-2.65
$sig Z_0 (\Omega)$	none	46.5	45.4	_	49.0-50.5	47.3-51.9
	all	_	39.8	_	44.5-45.5 [†]	46.2-50.1 ⁺
hor C_{12} (pF/cm)	none	0.188	0.145	0.143	0.096-0.131	_
vert C_{12} (pF/cm)	none	0.070	0.027	0.037	0.024-0.028	_
diag C_{12} (pF/cm)	none	0.038	0.014	_	0.011-0.015	_
hor C_{12} (pF/cm)	all	_	0.014	0.031	_	_
hor $V_{NE}(\text{sat})$ (%)	none	4.23	3.64		2.9-3.0	2.18-2.57
vert $V_{NE}(sat)$ (%)	none	1.58	0.98		0.9 - 1.0	0.93-0.98
diag $V_{NE}(\text{sat})$ (%)	none	0.86	0.55	_	0.5	0.44-0.64

were corrected for by calculating C from the difference in total capacitance of two lines having different lengths. Nylon supports, which gave the models mechanical stability, caused slight increases in capacitance. Some of the measurements involved coupling capacitances that were difficult to measure accurately because they were small and subject to interference from objects external to the scale model. The horizontal coupling capacitance, with OLVs present, should therefore be given only a small weight.

From Table 2, it can be seen that the agreement between the signal-line capacitance calculated and measured on the scale model was within about 4%. If we consider the increases in capacitance as y-lines, vias, and then both are included, the calculated values are respectively 8.9%, 20.9%, and 24.3%, and the measured values are 10.4%, 16.8%, and 22.4%. For the vias, the agreement was not as good. Differences were attributed to the presence of an adjacent return via in the calculations; such vias were not present in the scale model and generally are more distant in actual TCMs. Further, vias were modeled as square, but were round in the scale model, as in TCMs.

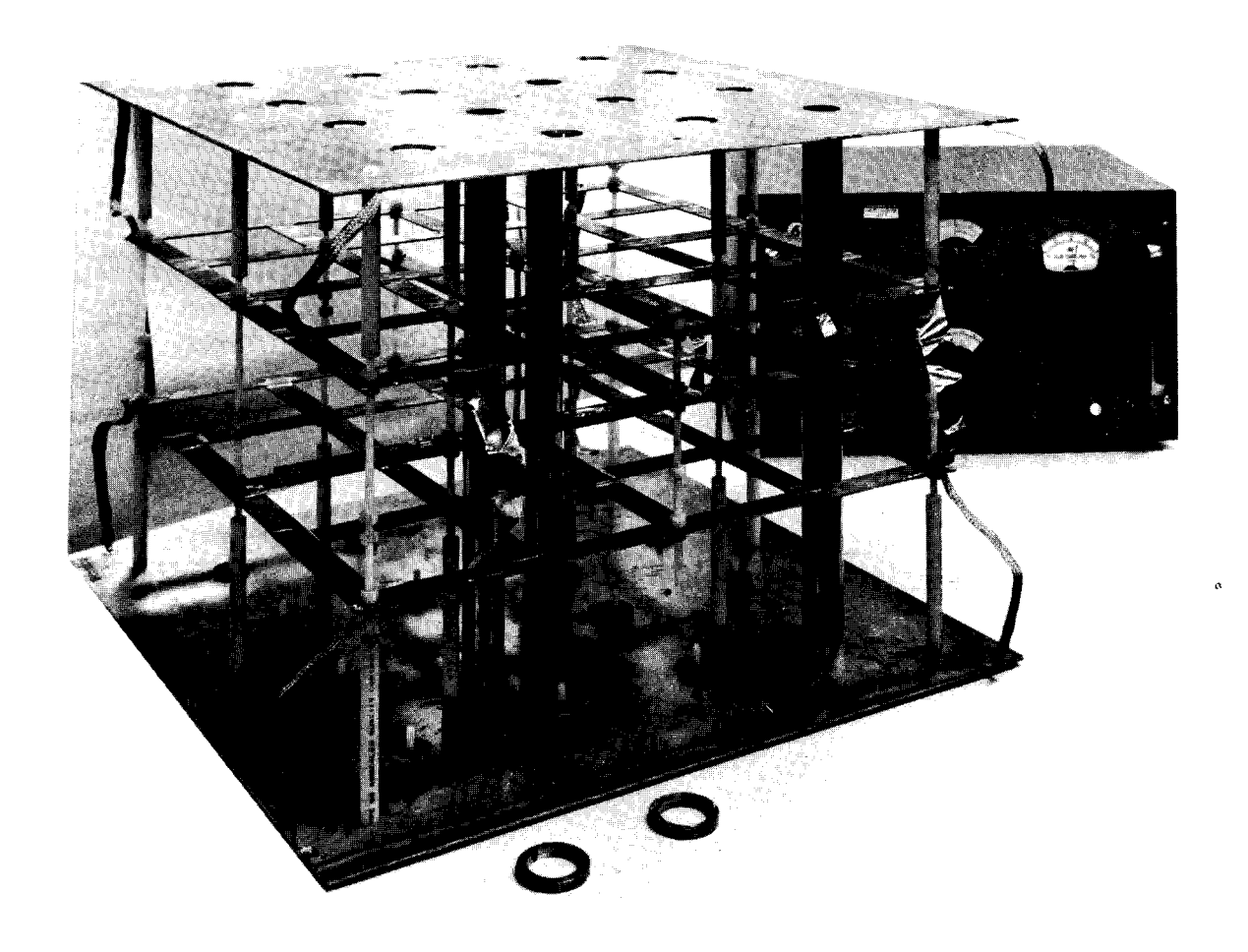
The last columns in Table 2 give the measurements on three samples of a specifically designed TCM test vehicle which were fabricated in 1979, and two more which were fabricated in 1985. Aside from the layout of their signal wiring (which was specially designed for parameter extraction), these test vehicles were actual TCMs, having electrical characteristics representative of TCMs in general. Capacitance was measured on roughly 100 signal lines, characteristic impedance was measured on about

two dozen signal lines, and signal-line coupling was measured on even fewer lines. The via capacitance was obtained by fabricating two lines that were identical except for the lengths of about ten vias that were deliberately attached as stubs; the via capacitance was found from the difference in measured capacitance of these two lines. Some lines (and vias) were specifically designed to run through regions having OLVs; others were isolated from the OLVs. In the electromagnetic analysis and scale models, the mesh lines were given the same width as the signal lines. Through physical sectioning of actual TCMs, however, we know this may not be realistic.

The measured signal-line capacitances were in good agreement with those predicted, but displayed less sensitivity to OLVs. The average signal-line capacitances, with and without OLVs, were 2.54 pF/cm and 2.31 pF/cm, respectively, for the 1979 test vehicles, and 2.57 pF/cm and 2.30 pF/cm, respectively, for the 1985 test vehicles. The measured impedances were higher than predicted, and their sensitivity to the presence of OLVs, especially for Z_0 in the 1985 data, were again smaller. The average characteristic impedances, corresponding to the above average capacitances, were 45.4 Ω , 49.8 Ω , 47.4 Ω , and 49.0 Ω , respectively. The measured coupling capacitances for the vertically and diagonally coupled lines agreed with those which were predicted, but those for horizontally coupled lines were smaller than either calculated or measured on the scale model.

The ranges in measured values were attributed to normal and expected process variations, especially in line cross section. Lines in TCMs are approximately oval

Adjacent return via. Via density of 70%.



and programme of

Scale model for signal-line characterization.

rather than rectangular, and have cross sections that may vary along their length. Furthermore, the presence of signal-line resistance and redistribution wiring introduces waveform effects that preclude the precise determination of Z_0 from measurements. Because of design constraints, vias and crossing lines could not be placed at each available site. The via density was 70%, meaning that 30% of the possible via positions were vacant. This factor partly explains the smaller OLV effects observed in the test vehicles.

Concluding remarks

The electromagnetic formulation has been applied to a number of canonical structures found in a TCM. As described, agreement well within engineering accuracy was observed when results were compared to measurements from scale models (which are reasonably close facsimiles of the structure analyzed). Agreement with measurements on the test vehicles was not quite as good, but this is attributed to normal tolerances in conductor size and shape. In a sensitivity analysis, where the geometric parameters would be varied and only the changes in the propagation parameters are needed, agreement would undoubtedly be far better.

The changes in propagation delay due to the presence of OLVs would have been difficult to predict by means of a circuit approach. In such an approach, capacitance and inductance are calculated independently, and thus may err in the same direction; if so, errors of several percent would yield a propagation delay that is also in error by

595

several percent. With delay varying typically by less than about 10%, as indicated in Table 1, a several percent error may be unacceptable. The use of a numerical grid which is sufficiently fine to provide satisfactory accuracy may not be practical with present-day computers. In the electromagnetic approach, the delay is calculated from the propagation constant associated with a traveling wave; it is the capacitance and inductance that are calculated using the delay, and not the other way around. Convergence studies performed in the references indicate that calculated delay may be accurate to within a fraction of one percent.

Though not considered here, such structures as stubs and right-angle bends of signal lines can be represented by a suitable unit cell and thus analyzed using this approach. In fact, the environment need not even be TCM-like; cables having helix-shaped shields and hollow waveguides can also be analyzed. Layered dielectrics can be included through the extension described in [22]. By employing a 3D array of hollow rectangular cells with appropriate surface impedances assigned to the cell walls [23], rooftop functions can also be used to model the polarization current [24] in finite-size dielectric regions. The above modifications allow the analysis of microstrip lines and dielectric waveguides [23].

In summary, the value of this approach lies in its full-wave nature and in its versatility. This single approach can be used to solve, within engineering accuracy, a large class of computer-package-related problems. It can save time and energy, since the alternative may be to search for or develop a multitude of different approaches and to piece together the needed results. Finally, and perhaps most significantly, this approach has provided, for the first time, an essentially complete electrical analysis of the TCM used in the IBM 3090 processor unit.

Appendix: Calculation of Z matrix

• Representation of rooftop function currents

The unit cell is divided into uniform intervals of length τ_x , τ_y , and τ_z along the x, y, and z directions, respectively, and fitted with full and half-rooftop function current elements, as discussed earlier and as indicated in Figure 3. The current in the unit cell is approximated as a linear combination of these rooftop functions multiplied by the phase factor e^{-jk_xx} . The following are unit vectors directed along a positive axis direction and associated with the rooftop function having index α , where $1 \le \alpha \le P'$ and P' is the total number of rooftop functions. Let $\mathbf{a}_{u\alpha}$ be along the direction of current flow, let $\mathbf{a}_{w\alpha}$ be normal to the plane containing the rooftop, and let $\mathbf{a}_{v\alpha}$ be orthogonal to both $\mathbf{a}_{u\alpha}$ and $\mathbf{a}_{w\alpha}$. We define variables, u, v, w, $\tau_{u\alpha}$, and $\tau_{v\alpha}$ in terms of x, y, and z as

$$u = \mathbf{a}_{u\alpha} \cdot (x\mathbf{a}_x + y\mathbf{a}_y + z\mathbf{a}_z),$$

$$v = \mathbf{a}_{v\alpha} \cdot (x\mathbf{a}_x + y\mathbf{a}_y + z\mathbf{a}_z),$$

$$w = \mathbf{a}_{w\alpha} \cdot (x\mathbf{a}_x + y\mathbf{a}_y + z\mathbf{a}_z),$$

$$\tau_{u\alpha} = \mathbf{a}_{u\alpha} \cdot (\tau_x\mathbf{a}_x + \tau_y\mathbf{a}_y + \tau_z\mathbf{a}_z),$$

$$\tau_{v\alpha} = \dot{\mathbf{a}}_{v\alpha} \cdot (\tau_x\mathbf{a}_x + \tau_y\mathbf{a}_y + \tau_z\mathbf{a}_z),$$
(A1)

where \mathbf{a}_x , \mathbf{a}_y , \mathbf{a}_z are unit vectors along the x, y, z directions, respectively. The use of the above variables, alone or in conjunction with the variables x, y, and z, allows for compact mathematical representations of the various field quantities. All the following expressions that involve u, v, and w may be converted to explicit functions of x, y, and z through the use of Equation (A1).

The volume current density **J** may be compactly expressed as

$$\mathbf{J} = \sum_{\alpha=1}^{P'} R_{\alpha}(x, y, z) e^{-jk_{x}x} I_{\alpha} \mathbf{a}_{u\alpha}, \tag{A2}$$

where $R_{\alpha}(x, y, z)$ is the rooftop function centered at $x = x_{\alpha}$, $y = y_{\alpha}$, $z = z_{\alpha}$, and I_{α} is the corresponding complex current coefficient.

Using the same notation as in Equation (A1) to define u_{α} , v_{α} , and w_{α} , e.g., $u_{\alpha} = \mathbf{a}_{u\alpha} \cdot (x_{\alpha}\mathbf{a}_{x} + y_{\alpha}\mathbf{a}_{y} + z_{\alpha}\mathbf{a}_{z})$, the rooftop function may be expressed as

$$R_{\alpha}(x, y, z) = q_{\tau}(u - u_{\alpha})p_{\tau}(v - v_{\alpha})\delta(w - w_{\alpha}),$$
 (A3)

where $q_{\cdot}(u)$ is the triangle function, defined as

$$q_{\tau}(u) = \begin{cases} 1 - \left| \frac{u}{\tau} \right| & -\tau \le u \le \tau, \\ 0 & \text{elsewhere:} \end{cases}$$
(A4)

 $p_{\bullet}(v)$ is the pulse function, defined as

$$p_{\tau}(v) = \begin{cases} 1 & -\tau/2 \le v \le \tau/2, \\ 0 & \text{elsewhere;} \end{cases}$$
 (A5)

and $\delta(w)$ is the Dirac delta function. Associated with each rooftop function α is a line interval, or integration path (see Figure 3), over which the electric field is tested. This interval is defined by its end points, located at $u = u_{1\alpha}$, $v = v_{\alpha}$, $w = w_{\alpha}$ and $u = u_{2\alpha}$, $v = v_{\alpha}$, $w = w_{\alpha}$, where

$$u_{1\alpha} = u_{\alpha} - \tau_{u\alpha}/2,$$

$$u_{2\alpha} = u_{\alpha} + \tau_{u\alpha}/2.$$
(A6)

As an example, for a rooftop function that lies in the y-z plane and has current directed along the y direction, $R_{\alpha}(x, y, z) = \delta(x - x_{\alpha})q_{\tau}(y - y_{\alpha})p_{\tau}(z - z_{\alpha})$, $u_{1\alpha} = y_{\alpha} - \tau_{\nu}/2$, and $u_{2\alpha} = y_{\alpha} + \tau_{\nu}/2$.

The above expressions apply only for a full rooftop function. For a half-rooftop function that is rising (falling) along the positive axis direction, the upper

(lower) bound of the inequality in the triangle definition (A4) is replaced by 0, and $u_{2\alpha}(u_{1\alpha})$ in Equation (A6) is set equal to u_{α} .

To find the general matrix term $Z_{\beta\alpha}$, where β is the row and α is the column, we consider the current associated with a single rooftop function α having $I_{\alpha}=1$ and centered at x=0, y=0, and z=0,

$$\mathbf{J} = g_{\alpha}(x, y) f_{\alpha}(z) e^{-jk_{x}x} \mathbf{a}_{u\alpha}. \tag{A7}$$

Here, the spatial dependencies of the rooftop function along the x and y directions have been lumped into $g_{\alpha}(x, y)$ and that along the z direction appears in $f_{\alpha}(z)$. Expressing $g_{\alpha}(x, y)$ as a Fourier series, we obtain

$$\mathbf{J} = \sum_{n,m} \mathbf{J}_{nm}(x, y, z)$$

$$= \sum_{n,m} G_{\alpha nm} e^{-j(2\pi n/d_1)x} e^{-j(2\pi m/d_2)y} f_{\alpha}(z) e^{-jk_x x} \mathbf{a}_{u\alpha}, \qquad (A8)$$

where

$$G_{\alpha nm} = \frac{1}{d_1 d_2} \int_0^{d_2} \int_0^{d_1} g_{\alpha}(x, y) e^{j(2\pi n/d_1)x} e^{j(2\pi m/d_2)y} dx dy,$$

and, as given earlier, d_1 and d_2 are the periodicities of the unit cell along the x and y directions, respectively.

Field equations employed

In the following, z is the normal direction and x and y lie in the transverse plane. The subscript t indicates that only the x and y components are involved, so that for a general vector \mathbf{A} , $\mathbf{A}_t = \mathbf{A} - A_z \mathbf{a}_z$. The electric field \mathbf{E} and the magnetic field \mathbf{H} are decomposed into their transverse and normal components. We define \overline{E}_u and \overline{E}_{tz} as the transverse components of the electric field produced by currents in the transverse and normal directions, respectively; \overline{E}_{zt} and \overline{E}_{zz} are the normal components of the electric field produced by currents in the transverse and normal directions, respectively. The magnetic field components \overline{H}_u , \overline{H}_{tz} , \overline{H}_{zt} , and \overline{H}_{zz} are similarly defined.

The electric and magnetic field corresponding to the current distribution of Equation (A8) must also be periodic functions multiplied by $e^{-jk_x x}$. In any region that is free of current sources, these fields, which must also satisfy the Helmholtz equation, can be expressed as

$$\mathbf{E} = \sum_{n,m} \mathbf{E}_{nm}(x, y, z)$$

$$= \sum_{n,m} \hat{\mathbf{E}}_{nm} e^{-jk_{xm}x} e^{-jk_{ym}y} e^{-jk_{znm}|z|}$$
(A10)

and

$$\mathbf{H} = \sum_{n,m} \mathbf{H}_{nm}(x, y, z)$$

$$= \sum_{n,m} \hat{\mathbf{H}}_{nm} e^{-jk_{xm}x} e^{-jk_{ym}y} e^{-jk_{znm}|z|},$$
(A11)

where

$$k_{xn} = k_x + \frac{2\pi n}{d_1},$$

$$k_{ym}=\frac{2\pi m}{d_2},$$

and

$$k_{znm} = (k_0^2 - k_{xn}^2 - k_{ym}^2)^{1/2},$$

and $\hat{\mathbf{E}}_{nm}$ and $\hat{\mathbf{H}}_{nm}$ are vectors that are independent of x, y, and z. The square root with the negative imaginary part is taken for k_{znm} . Each term corresponding to a given n and m is referred to as a space harmonic. As mentioned later, the current source will be placed in the plane z=0, so that the above expressions are valid in the source-free region, $z \neq 0$.

The electric field may be expressed in terms of the transverse component of the magnetic field [25] as

(A9)
$$-\frac{\partial}{\partial z} \mathbf{E}_{tnm}(x, y, z) = j\omega\mu_0 \left(\mathbf{1} + \frac{\nabla_{tnm}\nabla_{tnm}}{k^2} \right)$$
f the
$$\cdot \left[\mathbf{H}_{tnm}(x, y, z) \times \mathbf{a}_z \right]$$

$$+ \frac{\nabla_{tnm}J_{znm}(x, y, z)}{j\omega\varepsilon}$$
 (A12)

anc

$$E_{znm}(x, y, z) = \frac{1}{j\omega\varepsilon} \left\{ \nabla_{tnm} \cdot \left[\mathbf{H}_{tnm}(x, y, z) \times \mathbf{a}_z \right] - J_{znm}(x, y, z) \right\}, \tag{A13}$$

where $k = \omega \sqrt{\mu_0 \varepsilon}$, 1 is a unit dyadic such that $\mathbf{A} \cdot \mathbf{1} = \mathbf{1} \cdot \mathbf{A} = \mathbf{A}$, and ∇_{lnm} is a gradient operator, which, for the x and y dependencies given in Equations (A10) and (A11), can be expressed as

$$\nabla_{lnm} = -j(k_{xn}\mathbf{a}_x + k_{vm}\mathbf{a}_v). \tag{A14}$$

We also make use of the magnetic field boundary condition,

$$\mathbf{H}_{lnm}(x, y, z = 0^{+}) - \mathbf{H}_{lnm}(x, y, z = 0^{-})$$

$$= -\mathbf{a}_{z} \times \int_{0^{-}}^{0^{+}} \mathbf{J}_{nm}(x, y, z) dz, \tag{A15}$$

and that the divergence of the electric field is zero in any source-free region. The latter allows us to express the individual space harmonics of E_z in terms of those of E_z , as

$$E_{znm}(x, y, z) = \pm \frac{\nabla_{inm} \cdot \mathbf{E}_{inm}(x, y, z)}{jk_{-m}}, \qquad (A16)$$

where, in Equation (A16) and subsequently, the \pm sign corresponds to $z \ge 0$.

• Field calculations

The electric field components \overline{E}_{u} , \overline{E}_{tz} , \overline{E}_{zt} , and \overline{E}_{zz} will be found for the current given in Equation (A2) when $f_{\alpha}(z) = \delta(z)$; the corresponding fields for currents having pulse or triangle dependency along the z direction will be found by applying convolution.

To find \bar{E}_{tt} and \bar{E}_{zt} , $\mathbf{a}_{u\alpha}$ in Equation (A7) is set to either \mathbf{a}_{x} or \mathbf{a}_{y} . Using Equations (A8), (A11), and (A15), and noting that \bar{H}_{tt} is antisymmetric about z = 0, we find

$$\mathbf{H}_{inm}(x, y, z)$$

$$= \mp \frac{1}{2} G_{\alpha n m} e^{-jk_{\chi n} x} e^{-jk_{\gamma m} y} e^{-jk_{z n m} |z|} \mathbf{a}_{z} \times \mathbf{a}_{u \alpha}. \tag{A17}$$

Substituting Equation (A17) and the n, mth term of Equation (A10) into Equation (A12), replacing the operator ∂/∂_z by $\mp jk_{znm}$, and noting that the z-component of the current density has been set to zero, we obtain

$$\mathbf{E}_{lnm}(x, y, z) = -\frac{\omega \mu_0}{2k_{znm}} \left(\mathbf{1} + \frac{\nabla_{lnm} \nabla_{lnm}}{k^2} \right) \cdot \mathbf{a}_{u\alpha} G_{\alpha nm} e^{-jk_{xn}x} e^{-jk_{ym}y} e^{-jk_{znm}|z|} . \tag{A18}$$

The total field is obtained by summing over n and m. To find \overline{E}_{zi} , Equation (A18) is substituted into Equation (A16) and the result summed over n and m.

To find \overline{E}_{tz} , we set $\mathbf{a}_{u\alpha} = \mathbf{a}_z$ in Equation (A7). The Fourier series representation for \mathbf{J} (A8) is substituted into Equation (A12), and the resultant expression integrated along the z direction from $z=0^-$ to $z=0^+$. From Equation (A15), $\mathbf{H}_{tnm}(x, y, z)$ is continuous about z=0, so that the first term in Equation (A12) offers no contribution. Because \overline{E}_{tz} is antisymmetric about z=0, the left-hand side becomes $2\mathbf{E}_{tnm}(x, y, z=0^+)$. Comparing the result with the n, mth space harmonic in Equation (A10), evaluated at $z=0^+$, we find

$$\mathbf{E}_{tnm}(x, y, z) = \mp \frac{1}{2i\omega\varepsilon} \nabla_{tnm} G_{\alpha nm} e^{-jk_{xn}x} e^{-jk_{ym}y} e^{-jk_{znm}|z|}. \tag{A19}$$

Summing over n and m gives the desired result.

To find \overline{E}_{zz} , we again set $\mathbf{a}_{u\alpha} = \mathbf{a}_z$, but this time use Equation (A13). Because $f_{\alpha}(z) = \delta(z)$ in Equation (A7), only the first term in Equation (A13) contributes to the field in the source-free region, $z \neq 0$. But \overline{E}_{zz} may also be expressed, again in the source-free region, in terms of \overline{E}_{tz} through Equation (A16). Thus, \overline{E}_{zz} may be found for all

z by substituting Equation (A19) into Equation (A16), subtracting $J_{zmm}(x, y, z)/j\omega e$ and then summing over n and m. The first term in Equation (A13), through Equation (A15), is continuous at z=0; it introduces no mathematical difficulties. The second term in Equation (A13) must be included even though one may argue that the field could be tested just off the conductor's surface, where J is zero. Since we later truncate the infinite series expressions for all the field quantities, we must include J_z through its individual space harmonics, which exist over the entire x-y plane. Numerical difficulties have been observed when this term was omitted. In the context of dyadic greens functions, the first term corresponds to the principal-value part and the second term corresponds to the correction or depolarization factor [26].

If $f_{\alpha}(z)$ in Equation (A7) has a pulse or triangle dependency, the fields calculated for $f_{\alpha}(z) = \delta(z)$ are convolved with either $p_{\tau_z}(z)$ or $q_{\tau_z}(z)$, giving rise to factors having the form

$$\int_{-\tau_{z}}^{\tau_{z}} f_{\alpha}(z') [e^{-jk_{znm}(z-z')} U(z-z')$$

$$\pm e^{-jk_{znm}(z'-z)} U(z'-z)] dz', \tag{A20}$$

where U(z) is the unit step function and the sign is taken as positive for \overline{E}_u and \overline{E}_{zz} , and as negative otherwise. To account for the actual position of each rooftop function within the unit cell, x, y, and z in all the above expressions are replaced by $x-x_\alpha$, $y-y_\alpha$, and $z-z_\alpha$. This concludes the derivation of the electric field components.

To find $Z_{\beta\alpha}$, we then integrate the electric field and surface impedance components in the electric field boundary condition corresponding to rooftop function α over line interval β , giving

$$Z_{\beta\alpha} = \int_{u_{1\beta}}^{u_{2\beta}} \left[\mathbf{E}(x, y, z) - R_{s\alpha} R_{\alpha}'(x, y, z) e^{-jk_{x}x} \mathbf{a}_{u\alpha} \right] \cdot \mathbf{a}_{u\beta} du, \tag{A21}$$

where $u_{1\beta}$ and $u_{2\beta}$ are given by Equation (A6). The integration above is over the unit cell,

$$R'_{\alpha}(x, y, z) = \begin{cases} q_{\tau_{u\alpha}}(u - u_{\alpha})p_{\tau_{v\alpha}}(v - v_{\alpha}) & w = w_{\alpha}, \\ 0 & w \neq w_{\alpha}, \end{cases}$$
(A22)

and the terms in Equation (A21) are evaluated at

$$v = v_{\beta}$$
 and $w = w_{\beta}$.

The factor (A22) must be so defined because J in Equation (A2) is the volume current density and not the surface current density J_c appearing in Equation (2). The

598

factor $R_{s\alpha}$ is the sheet impedance for the conductor associated with rooftop function α and also appears in the electric field boundary condition (2); $R_{s\alpha}$ is given in Ω per square and allows for conductor loss. As discussed in the text, corresponding half-rooftop functions are combined to form corner functions. This operation reduces the matrix order by the number of corner functions formed, from P' to P. The eigenvalue equation (3) is then solved for k_x and for the P current coefficients I_{α} , which constitute the current eigenvector I of Equation (3). The current density is found through Equation (A2).

The derivation just given does not culminate here in the explicit formulas for the Z matrix elements. Because of the many possible relative orientations between the rooftop functions and line intervals, factor (A20) and its subsequent integration in Equation (A21) give rise to dozens of different expressions. As such, too much space would be required to give explicit formulas.

To find the characteristic impedance Z_0 , S additional line intervals are defined. These line intervals lie in the plane $x = \hat{x}$ and form a continuous path from the signal line to a suitable point on the reference conductor. The voltage difference V corresponding to this path may be expressed as

$$V = -\sum_{\beta=P+1}^{P+S} \sum_{\alpha=1}^{P} Z'_{\beta\alpha} I_{\alpha}, \qquad (A23)$$

where $Z'_{\beta\alpha}$ are the matrix elements after the half-rooftop functions have been combined to form corner functions. The total signal-line current may be expressed as

$$I_{\mathsf{T}} = \int \int \mathbf{J} \cdot \mathbf{a}_{x} \, dy \, dz, \tag{A24}$$

where the integration is performed over the signal-line cross section, and J, which is given by Equation (A2), is evaluated at $x = \hat{x}$. We define the characteristic impedance as $Z_0 = V/I_T$. Though V and thus Z_0 are uniquely defined only in TEM structures, they display only minimal spatial variations in typical computer package structures. As such, they are generally appropriate and useful parameters.

The infinite series that appear in all the $Z'_{\beta\alpha}$ elements are convergent (absolute convergence has been demonstrated for a subset of these elements in [14]). Good results have been obtained when the infinite series are truncated according to the following ratios of periodicity to subdivision size:

$$|n| \le \frac{d_1}{\min(\tau_x, \tau_z)}$$
 and $|m| \le \frac{d_2}{\min(\tau_y, \tau_z)}$, (A25)

where τ_x , τ_y , τ_z are the subdivision intervals discussed earlier and shown in Figure 3. For a structure composed exclusively of conductors having zero thickness along the

z direction, the denominators in Equation (A25) are replaced by τ_v and τ_v , respectively.

Acknowledgments

The author expresses deep appreciation to Sam Diehl, of the IBM facility in Hopewell Junction, New York, for fabricating the scale models which were used in this study, and for carrying out all the measurements on both the scale models and test vehicles. He also wishes to express his appreciation to Alina Deutsch and Gerard Kopcsay, both of the Thomas J. Watson Research Center, for using the electromagnetic approach in some of their analyses and providing valuable feedback. The author also extends a special thanks to Albert Ruehli of the Thomas J. Watson Research Center for many conversations over the years on package analysis. Lastly, the author thanks Professor Henry Bertoni of the Polytechnic University of New York for numerous discussions on wave propagation and other electromagnetic effects related to the work described in this paper.

References

- D. P. Seraphim and I. Feinberg, "Electronic Packaging Evolution in IBM." IBM J. Res. Develop. 25, 617-629 (1981).
- A. J. Blodgett and D. R. Barbour, "Thermal Conduction Module: A High-Performance Multilayer Ceramic Package," IBM J. Res. Develop. 26, 30–36 (1982).
- Donald P. Seraphim, "A New Set of Printed-Circuit Technologies for the IBM 3081 Processor Unit," IBM J. Res. Develop. 26, 37-44 (1982).
- E. E. Davidson, "Electrical Design of a High Speed Computer Package," IBM J. Res. Develop. 26, 349-361 (1982).
- W. T. Weeks, "Calculation of Coefficients of Capacitance of Multiconductor Transmission Lines in the Presence of a Dielectric Interface," *IEEE Trans. Microwave Theory Tech.* MTT-18, 35-43 (1970).
- W. T. Weeks, L. L. Wu, M. F. McAllister, and A. Singh, "Resistive and Inductive Skin Effect in Rectangular Conductors," *IBM J. Res. Develop.* 23, 652–660 (1979).
- A. E. Ruehli and P. A. Brennan, "Efficient Capacitance Calculations for Three Dimensional Multiconductor Systems," *IEEE Trans. Microwave Theory Tech.* MTT-21, 76–82 (1973).
- A. E. Ruehli, "Inductance Calculations in a Complex Integrated Circuit Environment," *IBM J. Res. Develop.* 16, 470–481 (1972).
- A. E. Ruehli, "Equivalent Circuit Models for Three-Dimensional Multiconductor Systems," *IEEE Trans. Microwave Theory Tech.* MTT-22, 216–221 (1974).
- S. Ramo, J. R. Whinnery, and T. Van Duzer, Fields and Waves in Communication Electronics, John Wiley & Sons, Inc., New York, 1965.
- R. F. Harrington, Field Computation by Moment Methods, Macmillan Publishing Co., New York, 1968.
- A. W. Glisson and D. R. Wilton, "Simple and Efficient Numerical Methods for Problems of Electromagnetic Radiation and Scattering from Surfaces," *IEEE Trans. Antenn. Propagat.* AP-28, 593-603 (1980).
- R. E. Collin, Field Theory of Guided Waves, McGraw-Hill Book Co., Inc., New York, 1960, Ch. 9.
- B. J. Rubin and H. L. Bertoni, "Reflection from a Periodically Perforated Plane Using a Subsectional Current Approximation," *IEEE Trans. Antenn. Propagat.* AP-31, 829-836 (1983).

- B. J. Rubin and H. L. Bertoni, "Waves Guided by Conductive Strips Above a Periodically Perforated Ground Plane," *IEEE Trans. Microwave Theory Tech.* MTT-31, 541-549 (1983).
- B. J. Rubin, "The Propagation Characteristics of Signal Lines in a Mesh-Plane Environment," *IEEE Trans. Microwave Theory* Tech. MTT-32, 522-531 (1984).
- B. J. Rubin and H. L. Bertoni, "Scattering from a Periodic Array of Conducting Bars of Finite Surface Resistance," *Rad. Sci.* 20, 827–832 (1985).
- B. J. Rubin, "Scattering from a Periodic Array of Apertures or Plates Where the Conductors Have Arbitrary Shape, Thickness, and Resistivity," *IEEE Trans. Antenn. Propagat.* AP-34, 1356– 1365 (1986).
- B. J. Rubin, "Modeling of Arbitrarily Shaped Signal Lines and Discontinuities," *IEEE Trans. Microwave Theory Tech.* 37, 1057–1060 (1989).
- G. Arjavalingam and B. Rubin, "Electrical Considerations for Interconnections Inside a Computer," Fiber Optic Datacom and Computer Networks, Society of Photo-Optical Instrumentation Engineers, Vol. 991, 12-21 (1988).
- A. Feller, H. R. Kaupp, and J. J. DiGiacomo, "Crosstalk and Reflections in High-Speed Digital Systems," AFIPS Conf. Proc., Fall Joint Computer Conf. 27, 511-525 (1965).
- C. H. Chan and R. Mittra, "The Propagation Characteristics of Signal Lines Embedded in a Multilayered Structure in the Presence of a Periodically Perforated Ground Plane," *IEEE Trans. Microwave Theory Tech.* 36, 968-975 (1988).
- B. J. Rubin, "Electromagnetic Modeling of Waveguides Involving Finite-Size Dielectric Regions," *IEEE Trans. Microwave Theory Tech.* 38, 807–812 (1990).
- D. H. Schaubert, D. R. Wilton, and A. W. Glisson, "A Tetrahedral Modeling Method for Electromagnetic Scattering by Arbitrarily Shaped Inhomogeneous Dielectric Bodies," *IEEE Trans. Antenn. Propagat.* AP-32, 77-85 (1984).
- L. B. Felsen and N. Marcuvitz, Radiation and Scattering of Waves, Prentice-Hall, Inc., Englewood Cliffs, NJ, 1973, Sec. 2.2.
- A. D. Yaghjian, "Electric Dyadic Green's Functions in the Source Region," *Proc. IEEE* 68, 248–263 (1980).

Received April 21, 1989; accepted for publication November 20, 1989

Barry J. Rubin IBM Research Division, Thomas J. Watson Research Center, P.O. Box 218, Yorktown Heights, New York 10598. Dr. Rubin received a Bachelor's degree in electrical engineering from the City College of New York in 1974. He then joined IBM at its East Fishkill facility in Hopewell Junction, New York. In 1978, he received an M.S. from Syracuse University, and, in 1982, a Ph.D. from the Polytechnic Institute of New York, both in electrical engineering. Dr. Rubin has worked on power transistor design, CCD technology, circuit design, and, since 1976, on electrical package analysis. He has been closely involved in the following aspects of TCM packages: signal propagation, coupled and delta-I noise, and verification of modeling. In 1986, he joined the Thomas J. Watson Research Center, where he is currently involved in the electromagnetic modeling of computer packages. Dr. Rubin has received two IBM Invention Achievement Awards.